Field-Induced Negative Differential Spin Lifetime in Silicon

Jing Li, Lan Qing, Hanan Dery, and Ian Appelbaum

Field-induced negative differential spin lifetime in silicon

Jing Li,[1] Lan Qing,[2] Hanan Dery,[2,3] and Ian Appelbaum[1,*]

[1] Department of Physics and Center for Nanophysics and Advanced Materials,
University of Maryland, College Park, MD 20742
[2] Department of Physics and Astronomy, University of Rochester, Rochester, NY 14627
[3] Department of Electrical and Computer Engineering, University of Rochester, Rochester, NY 14627

We show that the electric field-induced thermal asymmetry between the electron and lattice systems in pure silicon substantially impacts the identity of the dominant spin relaxation mechanism. Comparison of empirical results from long-distance spin transport devices with detailed Monte Carlo simulations confirms a strong spin depolarization beyond what is expected from the standard Elliott-Yafet theory even at low temperatures. The enhanced spin-flip mechanism is attributed to phonon emission processes during which electrons are scattered between conduction band valleys that reside on different crystal axes. This leads to anomalous behavior, where (beyond a critical field) reduction of the transit time between spin-injector and spin-detector is accompanied by a counterintuitive reduction in spin polarization and an apparent *negative* spin lifetime.

In compound semiconductors, the eventual reduction in drift velocity of conduction electrons with increasing applied electric field is known as negative differential mobility or the Gunn effect [1, 2]. In this field regime (typically several kV/cm), hot electrons scatter into low-lying secondary energy minima in the conduction band where the effective mass is larger, reducing their kinetic energy. The multivalley band structure of silicon also allows for the existence of this phenomenon but only at low temperatures; for all $T > 30$ K, the drift velocity increases and eventually saturates with increasing applied field [3],[4]. Therefore, at elevated temperatures the time-of-flight of conduction electrons across the Si channel of a transport device drops monotonically with increasing electric field. If electrons are initially spin polarized, then the accepted Elliott-Yafet spin relaxation theory suggests that the spin depolarization during transport is dependent only on the time-of-flight. In this theory the spin and momentum relaxation times are proportional [5, 6], so the resulting spin polarization increases with electron drift velocity. Indeed, we have confirmed this expectation in previous experiments where low and moderate applied fields (< 1 kV/cm) were used in studying the extraordinarily long spin lifetime [7, 8], and in demonstrating spin injection and detection in ferromagnet-silicon hybrid systems [9, 10].

In this Letter, we experimentally demonstrate an unexpected dependence of the spin polarization on the electric field in silicon at $T \geq 30$ K in high electric fields. With increasing field, the spin polarization of detected electrons first increases as expected from the Elliott-Yafet static lifetime model; however, above 2 kV/cm it starts to decrease, showing a Gunn-effect dependence akin to a negative differential spin lifetime without any simultaneous negative differential charge (spin) mobility. The origin of this counterintuitive behavior is then elucidated by Monte Carlo simulations and a quantitative analytical description: When the electron ensemble is out of thermal equilibrium with the lattice, an efficient spin relaxation mechanism becomes accessible due to field-induced intervalley scattering. We quantify the spin relaxation time as a function of both the lattice and electron ensemble temperature. The latter provides a means to determine the dependence of spin relaxation in silicon on the electric field. It enables the optimization of spintronics devices [11], as we can choose an electric field that maximizes the signal in spin transport.

Coherent spin precession and spin valve measurements were performed to observe the nonequilibrium depolarization effect and to quantify the negative differential region of spin lifetime. In both experiments, we employed all-electrical devices in which spin-polarized electrons (aligned with the in-plane magnetization direction of a ferromagnetic thin-film source) are tunnel injected through a Schottky metal contact and into a 225 μm - thick wafer of nominally undoped Si(100) [12]. The electrons then drift across the wafer thickness due to an applied electric field, and are collected by a second ferromagnetic film where their spin is analyzed using a ballistic spin detection scheme. The results presented below do not depend on the injection and detection techniques but only on the spin and charge transport characteristics of the Si channel. We therefore include all device-specific description in the supplemental material [13], and refer the interested reader to Refs. [7, 9, 10] for further details.

The time-of-flight distribution of the electron current can be recovered from quasistatic spin precession measurements by applying an external magnetic field, B, perpendicular to the injected spin direction but parallel to the electric field [14]. This magnetic field induces spin precession at frequency $\omega = g\mu_B B/\hbar$, where g is the electron g-factor, μ_B is the Bohr magneton, and $\hbar$ is the reduced Planck constant. We denote the time-of-flight distribution by $D(t)$ where its mean and standard deviation are, respectively, measures of the average transit time and of diffusion and dephasing effects in the channel. The signal contribution from the spin component parallel to the detector magnetization of an electron ar-
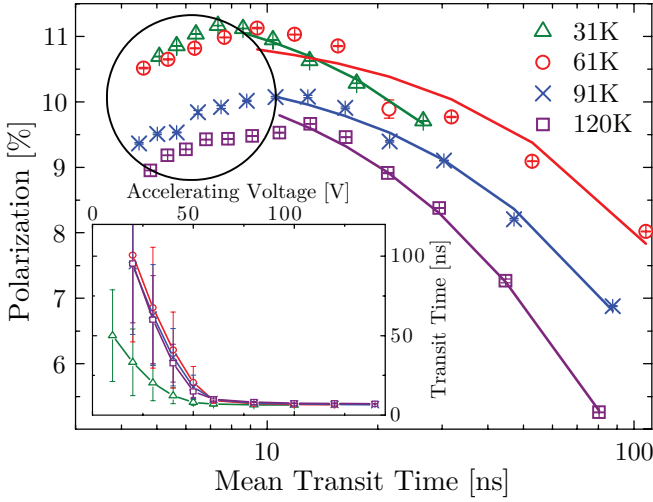
FIG. 1. Measured spin current polarization after transport across a 225-micron-thick intrinsic silicon device as a function of transit time in the silicon channel. Solid lines indicate exponential fits to the low-field (long transit time) data and indicate long spin lifetimes in that regime. Effects of spin depolarization from electric-field-induced spin relaxation are evident at high-fields (short transit time; circled data). Inset: Average transit time as a function of the applied voltage for various temperatures. Error bars indicate the transit time uncertainty (extracted from the width of the time-of-flight distribution).

riving at the detector in the time interval $[t, t + dt]$ is therefore $D(t) \cos \omega t \, dt$. The variation in quasistatic detected signal is then $D(\omega) \propto \int_0^\infty D(t) \cos \omega t \, dt$; by measuring as a function of applied perpendicular magnetic field, one can map the precession frequency dependence of the detected signal. Finally, the empirical time-of-flight distribution is recovered without any model fitting by the inverse Fourier transform of $D(\omega)$ [8]. The inset to Fig. 1 shows the average transit time across the silicon channel extracted from this distribution as a function of applied voltage for several temperatures. Clearly, increasing the internal electric field with applied voltage reduces the transit time until the onset of velocity saturation for voltages $\gtrsim 60$ V (electric field ~ 2.7 kV/cm) [4]. It is important to note that no negative differential mobility is seen [13].

To measure the spin polarization of collected electrons, we have performed independent spin-valve measurements as a function of the electric field. Here, a small external magnetic field of ≈ 2 mT is applied along the source magnetization axis and thus no spin precession is induced. The final spin polarization after transport is extracted by the ratio $\mathcal{P} = (I_P - I_{AP})/(I_P + I_{AP})$, where I_P is the measured signal current in a configuration where the in-plane injector and detector magnetization directions (and hence spin initialization and measurement axes) are parallel, and I_{AP} is for antiparallel configuration. The details of the spin-valve and time-of-flight spectroscopies

are presented in the supplemental material [13].

Figure 1 shows the measured polarization as a function of the average transit time (τ_{tr}). One expects that this polarization depends on τ_s, the spin relaxation time in the Si channel, as $\mathcal{P} = \mathcal{P}_0 e^{-\tau_{tr}/\tau_s}$, where $\mathcal{P}_0$ (limited by the spin-injection and detection efficiencies of the device) is the optimal attainable value. The figure shows that at long transit times, the polarization does indeed increase with reducing the transit time, as expected from the Elliott-Yafet theory. However, at short transit times (circled data) the trend is unexpectedly opposite. This observation of a nonmonotonic spin polarization Gunn effect is the main experimental result of this Letter.

The origin of this phenomenon is a transition to a previously-ignored regime where electric field directly enables a spin relaxation pathway. The field-induced momentum relaxation enhancement, as implied by the drift velocity saturation shown in the inset to Fig. 1, is evidently smaller than the spin relaxation enhancement. Applying the accepted Elliott-Yafet theory (proportionality of spin and momentum relaxation times) would therefore lead to the false conclusion that the rising polarization with initially increasing transit time is indicative of an unphysical *negative* spin lifetime.

We have performed Monte Carlo simulations in order to elucidate the charge transport and spin relaxation of conduction electrons heated by the electric field ("hot" electrons). A full description of the numerical procedure is provided in the supplemental material [13], and here we summarize the important features. Momentum relaxation mechanisms are modeled by electron-phonon interactions (both intravalley and intervalley processes) and intravalley electron scattering from ionized impurities [15]. Ellipsoidal energy bands $\epsilon(\mathbf{k})$ are used to model the equivalent six conduction band valleys [16]. Between scattering events, electrons are treated as classical particles accelerated by the electric field. Typically, an out-of-equilibrium electron distribution reaches its steady state within 1 ns regardless of the initial condition. Figure 2(a)-(b) show the corresponding drift velocity and mean energy as a function of applied electric field. Hot (cold) valleys refer to the four (two) valleys whose axis is perpendicular to (collinear with) the electric field. The mean energy in a hot (cold) valley is higher (lower) due to the different projections of electric field on the ellipsoidal energy bands.

The spin relaxation of electrons with distribution $f(\mathbf{k})$ is calculated by integration of the spin-flip matrix elements due to electron-phonon interaction [6, 17]:

$$\frac{1}{\tau_{s,\nu}} = \frac{2\pi\hbar}{\mathcal{D}} \int d^3\mathbf{k} \frac{\partial f(\mathbf{k})}{\partial \epsilon(\mathbf{k})} \int \frac{d^3\mathbf{k}'}{(2\pi)^3} \left\{ \left| M_\nu^{sf}(\mathbf{k}, \mathbf{k}') \right|^2 \frac{1}{\varrho \, \Omega_\nu(\mathbf{q})} \right.$$
$$\left. \times \left[\sum_\pm (n_{\nu,\mathbf{q}} + \tfrac{1}{2} \pm \tfrac{1}{2}) \delta\left(\epsilon(\mathbf{k}') - \epsilon(\mathbf{k}) \pm \Omega_\nu(\mathbf{q})\right) \right] \right\}. \quad (1)$$
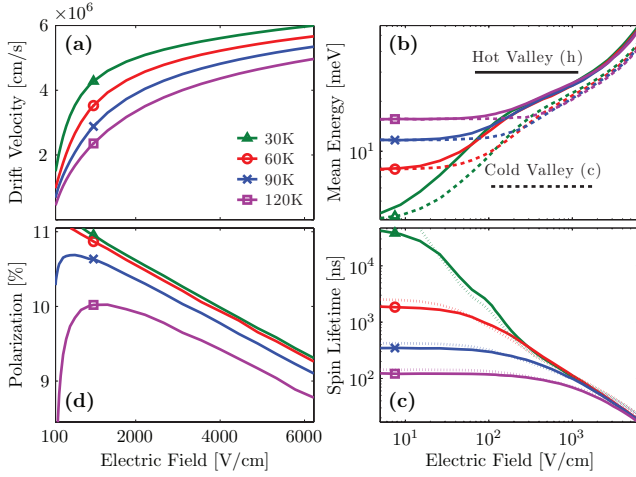
This expression is valid for Boltzmann statistics [18].

FIG. 2. (a) Electron drift velocity, (b) mean energy, (c) spin relaxation time and (d) final polarization as a function of electric field, calculated from numerical integration of the distribution obtained from Monte Carlo simulation. These behaviors persist up to room temperature in our simulations [13]. The dotted lines in (c) denote Eq. (2).

$\mathcal{D} = \int [\partial f(\mathbf{k})/\partial \epsilon(\mathbf{k})] d^3\mathbf{k}$ normalizes the integration. The term in the braces corresponds to the electron-phonon interaction which is the dominant spin relaxation mechanism in our nearly intrinsic sample. In heavily doped Si channels, on the other hand, additional scattering with impurities would lead to shorter spin lifetimes [19–21]. $\varrho = 2.33$ g/cm^3 is the crystal density and ν is the phonon mode. $\mathbf{q} = \mathbf{k} - \mathbf{k}'$, $\Omega_\nu(\mathbf{q})$ and $n_{\nu,\mathbf{q}}$ denote the phonon wavevector, energy and Bose-Einstein distribution, respectively. The $+(-)$ refers to phonon emission (absorption) processes. $M_\nu^{sf}(\mathbf{k}, \mathbf{k}')$ is the spin-flip matrix element between electronic states in the lower conduction band, which can be explicitly given for various processes [13, 17]. For the substantial f-process in which electrons are scattered between valleys of different crystal axes, the phonon wavevector resides on the Σ axis. The dominant phonon modes for spin relaxation are Σ_1 and Σ_3 with respective phonon energies of $\Omega_{f,1} \approx 47$ meV and $\Omega_{f,3} \approx 23$ meV. The spin-flip matrix element can then be written as $\left| M_{f,i}^{sf}(\mathbf{k}, \mathbf{k}') \right| = C_i D_i \Delta_x' / E_{g,x}$. We have the spin-orbit coupling parameter $\Delta_x' \approx 4.0$ meV, which pertains to the X point where the band gap is $E_{g,x} \approx 4.3$ eV. The scattering parameter $D_1 \approx 12$ eV/Å ($D_3 \approx 5$ eV/Å) is associated with a phonon mode of $\Sigma_{1(3)}$ symmetry. $C_1 = 2$ and $C_3 = 1$ if one of the involved valleys is along $\pm z$ (collinear with the spin-quantization axis) or $C_1 = 0$ and $C_3 = \sqrt{2}$ otherwise.

The solid lines in Fig. 2(c) show the simulated spin lifetime (numerically integrating Eq. (1) with $f(\mathbf{k})$ taken from the Monte Carlo hot-electron distributions). Figure 2(d) shows the resulting spin polarization $\mathcal{P}_0 \exp(-\tau_{tr}/\tau_s)$, where $\mathcal{P}_0 = 0.115$ is chosen to fit the experimental injection and detection efficiencies. The average transit time τ_{tr} is calculated from the drift velocity after transport across 225 μm. At low fields, the polarization rises with electric field since the increase of drift velocity surpasses the decrease of spin relaxation time. As the drift velocity begins to saturate in high fields, the polarization drops slowly due to the enhanced reduction of the spin relaxation time. This dependence of spin polarization on the electric field agrees well with the experimental results and reproduces the Gunn-type behavior (here shown as a function of the field).

To better understand the observed effect we first discuss the charge transport. Fig. 3(a) shows the Monte Carlo steady-state energy distributions in hot and cold valleys at 30 K and 4 kV/cm. Each of these distributions is well approximated by a two-component heated Maxwellian. In the low energy part, the effective temperature of the electron distribution can be extracted from the mean energy $\frac{3}{2}k_B T_e$, shown in Fig. 2(b). In the high energy tail, it is approximated by $T_e' = T + \gamma(T_e - T)$ where T is the lattice temperature and $\gamma \approx 0.9$ mimics the following cooling effect [13]: When electrons gain enough energy they deliver to the lattice a few tens of meV by emission of short-wave phonon modes. The sharper decay at the high-energy tails in Fig. 3(a) starts around energies which correspond to phonon-modes of the f-process momentum scattering. Other than introducing efficient cooling of energetic electrons, this intervalley scattering allows for energy transfer between hot and cold valleys and it also leads to saturation of the drift velocity (inset of Fig. 1).

The intervalley scattering of hot electrons has a significantly larger role in spin than in charge transport. Specifically, only the spin-flip matrix element of an f-process involves a *direct* coupling of conduction orbitals from one valley with the valence orbitals of a perpendicular valley [17]. This direct coupling results in a wavevector independent spin-flip matrix element which is significantly larger than for the other processes. Therefore, one can consider only the f-process in studying the spin relaxation of hot electron distributions. We continue and solve Eq. (1) by replacing $f(\mathbf{k})$ with a heated Maxwellian. The effective lattice and hot electron parameters are denoted by $y_i = \Omega_{f,i}/k_B T$, $y_{i,\mu}' = \Omega_{f,i}/k_B T_{e,\mu}'$ where i refers to the phonon mode and $T_{e,\mu}'$ to the effective temperature of energetic electrons in a cold ($\mu = c$) or a hot ($\mu = h$) valley. The spin lifetime then reads [13]

$$\frac{1}{\tau_s} \approx \mathcal{C} \sum_{i=1,3}^{\mu=h,c} A_{i,\mu} n_\mu \frac{\exp(y_i - y_{i,\mu}') + 1}{\exp(y_i) - 1} \left(\frac{4}{3} y_{i,\mu}'^{-\frac{1}{2}} + \sqrt{2} \right), \quad (2)$$

where $\mathcal{C} = 0.023$ ns^{-1} is a constant related to the spin-orbit coupling parameter of the X point at the edge of the Brillouin zone. $A_{1,h} = 8\,(12)$, $A_{3,h} = 1.5\,(1.25)$, $A_{1,c} = 8\,(4)$ and $A_{3,c} = 0.5\,(0.75)$ are symmetry related parameters when the electric field is collinear with (perpendicular to) the spin-quantization axis. The n_c and
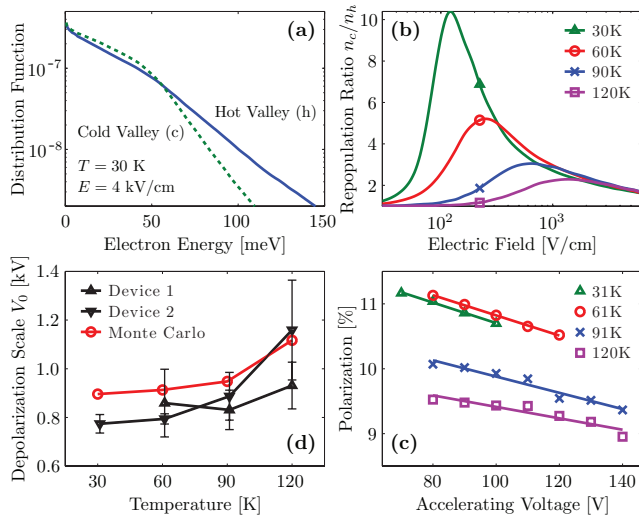
FIG. 3. (a) Electron distributions in hot (solid line) and cold (dashed line) valleys. The total electron density is 10^{12} cm^{-3}, the electric field is 4 kV/cm and the lattice temperature is 30 K. (b) Ratio between electron densities in cold and hot valleys as a function of the field. (c) Experimental depolarization at high-fields (extracted from Fig. 1). (d) Characteristic voltage scale for field-induced spin depolarization as a function of temperature.

n_h denote, respectively, the fractional population at cold and hot valleys where $2n_c + 4n_h = 1$. Figure 3(b) shows the repopulation ratio, n_c/n_h. The asymmetry in valley population is largest at intermediate fields since electrons that reside in hot valleys become energetic enough for intervalley scattering to cold valleys. At high fields, scattering in the opposite direction also becomes accessible and the valley population is more symmetrical ($n_c/n_h \approx 2$ in this regime). Substituting the extracted values of n_μ and $T'_{e,\mu}$ in Eq. (2) reproduces the spin relaxation of hot electrons as can be seen from the comparison between the dotted and solid lines in Fig. 2(c). At equilibrium conditions where $T'_{e,\mu} = T$ this mechanism is greatly suppressed (especially at low temperatures).

We can quantitatively compare the results of our calculations with empirical data by extracting a characteristic voltage scale V_0 for f-process-induced spin depolarization, where we approximate $\mathcal{P} \approx \mathcal{P}_0(1 - V/V_0)$ in the high electric-field regime. Fits to the measured spin polarization data are shown in Fig. 3(c), and the consistent temperature dependence of V_0 for several devices is shown in Fig. 3(d). The Monte Carlo prediction extracted from the high-field regime in Fig. 2(d) closely resembles the empirical values in both magnitude and lattice-temperature dependence due to the more efficient generation of intervalley scattering (and hence lower V_0) at lower temperatures. By taking the high-field limit of Eq. (2), one can write $V_0 \approx v_d/[d(\tau_s^{-1})/dE] \approx 1$ kV where v_d is the saturated drift velocity. This close correspondence confirms our interpretation of field-induced f-

process spin depolarization in the experiment, in a regime where acoustic-phonon-mediated scattering as well as scattering with states at the spin hot-spot [17, 22] are too small to account for this effect [13].

Finally, we note that a recent theoretical proposal suggesting that stochastic polarization fluctuations can be amplified by spin-dependent mobility [23] has also been termed a "spin Gunn effect". Our experiment and theory differ from this scheme in that the mobility and diffusion constants are spin independent, electron-electron collisions are negligible [24], and the physical origin of the effect is attributed to the signature of spin-orbit coupling on electron-phonon intervalley scattering. The phenomenon observed here, as in its charge-based counterpart, is due to a strong electric field-induced relaxation which leads to a qualitatively different spin transport regime distinct from expectations based on the Elliott-Yafet theory.

In conclusion, high electric fields present in silicon devices can substantially change the dominant physical mechanism of spin relaxation. In this regime, the Elliott-Yafet mechanism mediated by intravalley acoustic phonons is far outweighed by the depolarizing effects of inelastic scattering with intervalley f-process phonons created by the efforts of the system to recover thermal equilibrium. This behavior is expected to be critically important in the design of devices making use of spins to transmit information, especially when strong static electric fields are required [11]. Similarly, the derived dependence of the spin lifetime on the electric field is of fundamental importance to the design of semiconductor devices that make use of spin as an alternative degree of freedom [25–28].

[*] appelbaum@physics.umd.edu
[1] J. Gunn, IBM J. Res. Dev. **8**, 141 (1964).
[2] H. Kroemer, Proc. IEEE **52**, 1736 (1964).
[3] In $T \lesssim 30$ K and at electric fields around 100 V/cm, electrons predominantly scatter into valleys that are parallel to the field direction (where the effective mass is heavier). In larger fields or at higher temperatures electrons have enough energy to redistribute more evenly among the valleys and the effect disappears.
[4] C. Canali, C. Jacoboni, F. Nava, G. Ottaviani, and A. Quaranta, Phys. Rev. B **12**, 2265 (1975).
[5] R. Elliott, Phys. Rev. **96**, 266 (1954).
[6] Y. Yafet, in *Solid State Physics-advances in Research and Applications*, Vol. 14, edited by F. Seitz and D. Turnbull (Academic Press, New York, 1963).
[7] B. Huang, D. J. Monsma, and I. Appelbaum, Phys. Rev.

Lett. **99**, 177209 (2007).

[8] B. Huang and I. Appelbaum, Phys. Rev. B **82**, 241202 (2010).

[9] I. Appelbaum, B. Huang, and D. J. Monsma, Nature **447**, 295 (2007).

[10] B. Huang, L. Zhao, D. J. Monsma, and I. Appelbaum, Appl. Phys. Lett. **91**, 052501 (2007).

[11] H. Dery, Y. Song, P. Li, and I. Žutić, Appl. Phys. Lett. **99**, 082502 (2011).

[12] The thickness can be chosen arbitrarily, as long as the channel can be considered as bulk where the injected electrons achieve a steady-state distribution.

[13] See supplementary material at ... for technical details of the experiments, Monte Carlo simulation, and for useful quantitative expressions.

[14] The applied magnetic field is oriented perpendicular to in-plane magnetizations of the ferromagnetic source and detector films. These magnetization directions are not affected by the field due to their shape anisotropy.

[15] An impurity density of 10^{12} cm^{-3} is used to match the resistivity of the silicon wafers (4 kΩ·cm at room-temperature). At this low density, the transport parameters are practically independent on impurity scattering at high electric fields.

[16] C. Herring and E. Vogt, Phys. Rev. **105**, 1933 (1957).

[17] P. Li and H. Dery, Phys. Rev. Lett. **107**, 107203 (2011).

[18] Equation (1) is valid for Fermi-Dirac statistics only if the difference of chemical potentials between spin-up and spin-down populations is much smaller than $k_B T$.

[19] T. Sasaki, T. Oikawa, T. Suzuki, M. Shiraishi, Y. Suzuki, and K. Noguchi, Appl. Phys. Lett. **96**, 122101 (2010).

[20] T. Sasaki, T. Oikawa, M. Shiraishi, Y. Suzuki, and K. Noguchi, Appl. Phys. Lett. **98**, 012508 (2011).

[21] Y. Ando, K. Kasahara, K. Yamane, Y. Baba, Y. Maeda, Y. Hoshi, K. Sawano, M. Miyao, and K. Hamaya, Appl. Phys. Lett. **99**, 012113 (2011).

[22] J. L. Cheng, M. W. Wu, and J. Fabian, Phys. Rev. Lett. **104**, 016601 (2010).

[23] Y. Qi, Z.-G. Yu, and M. E. Flatté, Phys. Rev. Lett. **96**, 026602 (2006).

[24] I. D'Amico and G. Vignale, Europhys. Lett. **55**, 566 (2001).

[25] H. Dery, P. Dalal, L. Cywinski, and L. J. Sham, Nature **447**, 573 (2007).

[26] X. Lou, C. Adelmann, S. Crooker, E. Garlid, J. Zhang, S. Reddy, S. Flexner, C. Palmstrøm, and P. A. Crowell, Nature Phys. **3**, 197 (2007).

[27] J. Fabian, A. Matos-Abiague, C. Ertler, P. Stano, and I. Žutić, Acta Phys. Slovaca **57**, 565 (2007).

[28] B. Behin-Aein, D. Datta, S. Salahuddin, and S. Datta, Nature Nanotechnology **5**, 266 (2010).